Journal of Nuclear Medicine, published on November 13, 2020 as doi:10.2967/jnumed.120.253575

Poly(ADP-ribose)polymerase1: A potential molecular marker to identify cancer during colposcopy procedures.

Paula Demétrio De Souza França[1,2], Navjot Guru[1], Abigail R. Kostolansky[1,3], Audrey Mauguen[4], Giacomo Pirovano[1], Susanne Kossatz[1,5], Sheryl Roberts[1], Marcio Abrahão[2], Snehal G. Patel[6], Kay J. Park[7], Thomas Reiner[1,8,9,*], Elizabeth Jewell[6,*]

[1] Department of Radiology, Memorial Sloan Kettering Cancer Center, New York, NY, USA.

[2] Department of Otorhinolaryngology and Head and Neck Surgery, Federal University of São Paulo, SP, Brazil.

[3] Department of Chemistry, Princeton University, Princeton, NJ, USA.

[4] Department of Epidemiology and Biostatistics, Memorial Sloan Kettering Cancer Center, New York, NY, USA.

[5] Department of Nuclear Medicine, University Hospital Klinikum Rechts der Isar and TranslaTUM, Technical University Munich, Munich, Germany

[6] Department of Surgery, Memorial Sloan Kettering Cancer Center, New York, NY, USA.

[7] Department of Pathology, Memorial Sloan Kettering Cancer Center, New York, NY, USA.

[8] Department of Radiology, Weill Cornell Medical College, New York, NY, USA.

[9] Chemical Biology Program, Memorial Sloan Kettering Cancer Center, New York, NY, USA.

*EJ and TR contributed equally as co-senior authors

Short running title: PARP1 for cervical tumor identification

Correspondence should be addressed to:

*Thomas Reiner

1275 York Avenue

New York, NY, 10065

1-646-888-3461

reinert@mskcc.org

*Elizabeth Jewell

1275 York Avenue

New York, NY, 10065

1-646-888-3461

jewelle@mskcc.org

Keywords: PARPi-FL, cervical cancer, fluorescence-guided surgery, PARP1

Additional information.

Financial support. This work was supported by National Institutes of Health grants P30 CA008748, R01 CA204441 (TR), R43 CA228815 (TR), the Molecularly Targeted Intra-Operative Imaging Fund of Memorial Sloan Kettering Cancer Center, the Department of Surgery Funds, and the Memorial Sloan Kettering Imaging and Radiation Sciences

Program. The funding sources were not involved in study design, data collection and analysis, writing of the report, or the decision to submit this article for publication.

Key Points:

1.PARPi-FL is a topical fluorescent tracer that targets the PARP1 enzyme in the DNA repair chain, overexpressed in cancer.

2. After topical application, PARPi-FL signal can be picked up by a hand-held confocal microscope allowing cellular resolution of cervical lesions.

Manuscript Characteristics.

Word count: Abstract 203, Word total: 3676

# of Figures: 6 in Main text, 0 in Supplementary Information

# of Tables: 0 in Main text, 2 in Supplementary Information

# of References: 37 (Max 50)

Abstract

Despite efforts in prevention, cervical cancer still presents with a high worldwide incidence and remains a great problem in public health, especially in low-income countries. Screening programs, such as colposcopy with Papanicolaou testing, have greatly improved mortality rates. However, the agents currently used to delineate those lesions (topical application of acetic acid and/or Lugol's iodine) lack specificity and sometimes can lead to unnecessary biopsies or even cervical excisions. A tool to enable in vivo histology to quickly and quantitatively distinguish between tumor, dysplastic and healthy tissue would be of great clinical interest.

Here we describe the use of PARPi-FL, a fluorescent imaging agent that targets PARP1, a nuclear enzyme that is overexpressed in cancer when compared to the normal surrounding tissues. We exploit its use as an optical imaging agent to specifically target PARP1 expression, which was demonstrated to be higher in cervical cancer when compared to the normal surrounding tissue.

After its topical application on freshly excised cone biopsies, the nuclei of tumor cells emitted a specific fluorescent signal that could be visualized using a hand-held fluorescence confocal microscope.

This approach has the potential to improve in vivo identification of tumor cells during colposcopy examination allowing a rapid, non-invasive, and accurate histopathological assessment.

Introduction:

Globally, cervical cancer is still a widespread disease and ranks as the second most frequent cancer among young women (between 20 and 45 years of age) in low-income and lower-middle-income countries (1, 2), where access to healthcare providers and human papillomavirus (HPV) vaccination is scarce (2, 3). Several technologies to improve prevention, screening, and detection of cervical cancer have been recently described in the literature, including new imaging tools (4-7) and molecular tests for HPV detection (8, 9); however, they have yet to be approved for standard clinical practice. Visual inspection of the cervix after application of acetic acid and/or Lugol's iodine is still widely used as the standard screening method, especially in resource-limited places (4). Although broadly used, this technique presents variable sensitivity and specificity for detecting pre-cancerous lesions mostly due to observer bias (10). More consistent results using acetic acid and/or Lugol's iodine to guide biopsies are acquired with adequate provider training and continuous re-training (11). Besides this, staining with acetic acid and/or Lugol's iodine do not enable an in vivo cellular visualization of the cervix and are used mainly to guide biopsies. The final result depends on the histopathological analysis of the tissue, usually available only days after the procedure.

A tool to enable in vivo histology, to quickly and accurately distinguish between malignant, in situ (CIN) carcinomas and healthy tissue without the need of invasive biopsy, would be of great clinical interest. To address a possible solution and to perform in vivo, nontoxic, more accurate and faster diagnosis of cervical lesions, without the need of a biopsy, we turned to the topical application of PARPi-FL. PARPi-FL is a fluorescent

poly [ADP-ribose] polymerase 1 (PARP1) inhibitor, and a hand-held confocal microscope, to enable immediate identification of invasive and in situ carcinoma at a cellular level. PARPi-FL is derived from the scaffold of Olaparib, a PARP1 inhibitor that is currently being used mostly for the treatment of breast and ovarian cancer (12, 13). PARPi-FL penetrates the nuclei of cells and emits a fluorescent signal enabling its use as a surrogate of PARP1 expression (14).

A previous report in oral squamous cell carcinoma demonstrated that PARP1 expression gradually increases as the tissue accumulates molecular alterations (15). Besides this, it has also been reported that PARP1 overexpression in cancer cells is so remarkable that it enables tumor delineation in several malignancies (14-17). Importantly, studies have shown that PARPi-FL can be safely administered as a topical solution (15, 18) and has high tissue permeability (4.6 μm/s) accumulating within minutes in the nuclei of cancer cells (19), where it is retained for several hours allowing its use as a tumor stain. PARPi-FL use as an imaging tracer is well established and has been reported both preclinically (18-21) and clinically (15), for several other tumor types. In this study, we report PARP expression in cervical adenocarcinoma compared to the normal surrounding tissue. In addition, we performed experiments on both a swine animal model and on patients' ex vivo cone biopsies to investigate the feasibility of in vivo detection of cervical cancer during colposcopy procedures.

Materials and Methods

Chemicals. Commercially available compounds were used without further purification unless otherwise stated. Bio Ultra PEG 300, triethylamine (NEt_3) and trifluoroacetic acid (TFA) were purchased from Sigma-Aldrich (St. Louis, MO). HPLC and LC-MS grade acetonitrile (MeCN) were obtained from Fischer Scientific (Hampton, NH). Water (18.2 MΩ cm^{-1} at 25 °C) was obtained from an Alpha-Q Ultrapure water system from Millipore (Bedford, MA). PARP-NH precursor (4-(4-fluoro-3-(piperazine-1-carbonyl)benzyl)phthalazin-1(2H)-one) was purchased from AA blocks (San Diego, CA) and purified by HPLC before use and further synthesis. BODIPY-FL NHS-ester was purchased from Invitrogen, Carlsbad, CA without further purification. PARPi-FL was kept as a 1.5 mM stock solution in 100% BioUltra PEG 300 and diluted to the final working concentration for the respective experiments. All reactions were magnetically stirred, and room temperature refers to 20–25 °C. High performance liquid chromatography (HPLC) purification and analysis was performed on a Shimadzu UFLC HPLC system equipped with a DGU-20A degasser, an SPD-M20A UV detector, a LC-20AB pump system, and a CBM-20A communication BUS module.

PARPi-FL Synthesis. PARPi-FL was synthesized according to our previously described procedure (22). Briefly, BODIPY-FL NHS-ester (1.0 equivalent) was conjugated to 4-(4-fluoro-3-(piperazine-1-carbonyl)benzyl) phthalazin-1(2H)-one (1.0 equivalent) in the presence of Et_3N (5.0 equivalents) in acetonitrile for 4 h at room temperature. It was purified by preparative HPLC (Atlantis® T3 5 µm column 4.6 × 250 mm, 1 mL/min, 5 to

95% of acetonitrile (0.1% TFA) in 15 min) to afford PARPi-FL in 70–79% yield as a red solid. Analytical HPLC analysis (Waters' Atlantis T3 C18 5 μm 4.6 × 250 mm column) showed high purity (> 99%, t_R = 13.9 min) of the imaging agent. The identity of PARPi-FL was confirmed using ESI-MS (MS(+) *m/z* = 663.63 $[M + Na]^+$).

Animal Work. To demonstrate PARP1 expression in the basal cells of normal cervixes and to show that tissues would have PARPi-FL uptake, we developed an animal model using swine cervixes. Three Yorkshire female swine were purchased from Archer, Darlington, Maryland, USA. A cold knife cone biopsy was performed after euthanasia. The specimens were stained with PARPi-FL (tissue was submerged in a 100 nM solution – 1 μg of PARPi-FL in 15 mL of 30% PEG 300 in PBS for 5 minutes) and then imaged using a hand-held confocal microscope. After imaging, the specimens were routinely processed (formalin fixed, paraffin embedded) for hematoxylin and eosin (H&E) staining and PARP1 immunohistochemistry (IHC). All animal experiments were performed in accordance with protocols approved by the Institutional Animal Care and Use Committee (IACUC) of MSK and followed the National Institute of Health guidelines for animal welfare.

Handheld Confocal Fiberoptic Imaging. Images were acquired as previously described. Briefly, the FIVE2 (Optiscan, Victoria, Australia) hand-held confocal microscope acquires images by using a single channel for illumination and detection of PARPi-FL (488 nm excitation) and lens NA = 0.3 (similar to a 10× objective) with a field of view of 475 μm × 475 μm. The probe was in direct contact with the tissue to acquire

images. Different depths were assessed (Z axis, 0 μm – 400 μm). For all experiments, we used a band pass filter of 515 nm – 575 nm, 94 - 100% laser power, and a scanning speed of 1 frame per second. The depth in which the image was acquired is specified in each figure.

Patient Population. Seven banked cases of cervical adenocarcinoma (no tissue with CIN was included in this analysis) were acquired from the MSK tissue bank. In the operating room, freshly resected cone excisions (n=3) and a clitoral biopsy (n=1) were acquired. In all cases, research was performed under Institutional Review Board (IRB) approval and in accordance with the Declaration of Helsinki guidelines. Written informed consent had been obtained from all participants.

H&E Staining to Delineate Cervical Cancer Lesions. To delineate tumor vs. normal tissue and further correlate findings with IHC, slides were stained with H&E according to our previously described technique. Briefly, paraffin embedded sections (5 μm each) were obtained from the tissue bank at MSK and stained with H&E by the MSK Molecular Cytology Core facility. Slides were further scanned (Mirax, 3DHISTECH, Budapest, Hungary) to allow for digital histological analysis. All cases were reviewed by an experienced gynecologic pathologist who delineated viable tumor and normal tissue.

PARP1 immunohistochemistry. PARP1 IHC was performed on a consecutive slide according to our previously described procedure (18). Briefly, PARP1 immunohistochemistry was performed by automated Discovery XT processor (Ventana

Medical Systems, Tucson, AZ). The anti-PARP1 rabbit monoclonal antibody (46D11, Cell Signaling Technology, Danvers, MA) specifically binds both human and mouse PARP1 (0.4 µg/mL). Anti-PARP1 antibody was incubated for 5 hours, followed by 1 hour of incubation with biotinylated goat anti-rabbit IgG (PK6106, Vector Labs, Burlingame, CA) at 1:200 dilution. For IHC detection, a 3,3'-Diaminobenzidine (DAB) detection kit (Ventana Medical Systems, Tucson, AZ) was used according to the manufacturer's instructions, sections were counterstained with hematoxylin and cover-slipped with Permount (Fisher Scientific, Pittsburgh, PA). Incubating with a rabbit IgG instead of the primary antibody controlled for non-specific binding of the secondary antibody. H&E stained slides were used to delineate tumor and normal tissue. Those exact same areas were used for PARP1 quantification using the consecutive slide. PARP1 quantification was performed on digitalized slides according to our previously described procedure (15). Briefly, the threshold for signal intensity in the DAB (brown) and hematoxylin (blue - representing all tissue area) channels was determined using an automated script within the Image J analysis software for all samples used in the quantitative analyses. Color deconvolution was used to separate blue and brown signals and the threshold values were kept constant: 0 - 114 for DAB and 0 - 235 for hematoxylin. The relative PARP1 positive area was calculated by dividing the brown (DAB) area by the blue (total tissue area).

PARPi-FL Staining Procedure of Ex vivo Fresh Cervical Tissue. Staining was carried out on the whole, freshly excised cone biopsy specimen by submerging the tissue in a solution containing 1000 nM of PARPi-FL in 15 mL of 30% PEG 300 in PBS for 5 minutes (rapid staining protocol). The specimen was further washed in PBS for 1 min prior to

imaging. After imaging, the specimens were processed according to standard of care. A gynecological pathologist confirmed the histological results and provided an H&E slide and a slide for PARP1 IHC. Personnel that performed PARP staining and analyses were blinded from the sample type and from the pathologist's final report at the time of tissue analysis.

Quantification of PARPi-FL signal intensity. The quantification of PARPi-FL signal intensity was carried out on a tumor and normal areas using Fiji (ImageJ). The same window leveling was used for tumor and normal for each patient. 15 ROIs in tumor and 15 ROIs in the normal tissue were drawn. The intensity was calculated by averaging the values. Tumor to background ratio was calculated by dividing the average signal derived from tumor by the average intensity signal derived from the normal tissue.

Statistical analysis. Statistical analysis of PARP1 expression was performed using R v3.6.0 (R Core Team -2018, R Foundation for Statistical Computing, Vienna, Austria) and GraphPad Prism 8 (GraphPad Software, San Diego, CA). To compare PARP1 expression (ratio PARP1 expression / Total tissue area) between tumor, epithelium and deep tissue, we used a linear regression with random intercept in order to account for the correlation between measurements from a same patient. The linear regression was done on the logarithm transformation of the ratio (to ensure no negative prediction). Results with p-value ≤ 0.05 were considered statistically significant. Statistical analysis of PARPi-FL confocal fluorescence was performed using the Mann-Whitney test. Data points represent mean values, and error bars represent standard deviations.

Results

PARPi-FL imaging of swine cervical tissue with a hand-held confocal microscope. In order to analyze the value of handheld confocal microscopy in cervical tissue, we evaluated three cervical cone biopsies from healthy swine (Fig. 1A), taking advantage of the physiologic PARP1 expression in the healthy basal layer of the cervical squamous mucosa (Fig. 1B). After staining, we observed a relatively weak, but detectable PARPi-FL signal in the nuclei of the basal layer cells using the hand-held confocal microscope (Fig. 1C). Confocal imaging showed a highly organized tissue layer, with a homogeneous nuclear population of the same size and shape. The corresponding histological slides (H&E and PARP1 IHC) confirmed PARP1 expression in the nuclei of the basal layer of the cervical mucosa, which was present but weaker than what we observed in tumor tissue (Fig. 1B).

PARP1 is overexpressed in cervical cancer when compared to normal tissue – analysis of slides of banked tissue. Slides were cut from banked paraffin embedded tissue of cervical adenocarcinoma and were reviewed by a gynecologic pathologist to identify tumor and normal using H&E as gold standard. Immunohistochemistry was used for quantification of PARP1 levels within tumor and normal tissue. The data on PARP1 expression comes from 7 patients with cervical adenocarcinoma, each having between 11 and 39 measurements (median = 33). No premalignant lesions were analyzed in this cohort. We found that PARP1 was overexpressed in cancer and its expression was significantly higher when compared to the normal adjacent squamous mucosa (Fig. 2A).

Mean PARP1 expression in healthy deep cervical stroma was also shown to be lower compared to the normal squamous epithelium. This was expected, because of physiologic proliferation of the cervical epithelium. Importantly, the expression in the epithelium was significantly lower than in tumor areas allowing a clear differentiation between them (Fig.2B and Supplementary table 1). When accounting for the repeated measurements per patients, using 1 as a reference coefficient value on the statistic model, the ratio of the PARP1-positive area over the total tissue area was on average 95% lower (PARP1 positive area / Tissue area) in benign squamous epithelium as compared to tumor, and 99% lower (PARP1 positive area / Tissue area) in normal stroma as compared to tumor ($p < 0.001$, see Supplementary table 2). The ratio (PARP1 positive/ Total tissue area) in normal stroma was on average 77% lower than in benign squamous epithelium (95%CI: 0.18 to 0.30, $p < 0.001$). Fig. 2C demonstrates the ratio distribution in tumor, squamous epithelium and stroma.

Ex vivo PARPi-FL tumor detection in human cervical excisions and clitoral biopsy. After confirming feasibility of the technique in a preclinical large-animal model, we tested hand-held confocal microscopy using PARPi-FL in human cone biopsies inside the operating room. Three patients who were scheduled to undergo cone biopsy due to suspicious adenocarcinoma lesions had their surgical specimens stained and imaged prior to pathology assessment. Figure 3 visualize the study workflow. Patient 1 (Fig. 4A) harbored an adenocarcinoma at the transformation zone, extending to the ectocervix (dashed lines, Fig. 4A). Confocal imaging of the tumor area presented a disorganized pattern of cell nuclei with different sizes and shapes (arrows), yielding a fluorescent signal

of 83.57 ± 11.85 a.u. On the other hand, when imaging the normal mucosa, low PARPi-FL signal could be observed, fluorescent signal of 31.57 ± 14.82 a.u. We only observed a small number of sparse and small nuclei (arrows), which were visually distinct from tumor tissue. Each specimen underwent PARP1 IHC and the areas with increased PARP1 expression corresponded to the tumor seen on H&E. PARP1 expression was insignificant in the normal tissue, matching the observed levels of PARPi-FL. The tumor-to-background ratio (TBR) of fluorescence in the histologically proven lesion versus normal of the same tissue specimen/section of this patient is 2.65 (Fig. 4A). Patient 2 harbored an HPV-associated adenocarcinoma (dashed lines, Fig. 4B) located adjacent to a benign Nabothian cyst (represented by the number 2 on Figs. 4B), which can lead to overestimation of tumor volume on regular imaging. Confocal imaging of the tumor demonstrated cells with differently sized and shaped nuclei arranged in a highly disorganized manner. We did not observe any PARPi-FL uptake in the cyst wall or normal cervical mucosa. PARP1 expression corroborated the confocal imaging findings: Higher expression was seen in tumor, whereas almost no expression was present in the cyst or normal cervical mucosa. PARPi-FL emitted a signal of 105.8 ± 15.45 a.u. in tumor. The signal is significantly higher when compared to the normal adjacent mucosa (22.53 ± 2.95 a.u., $p < 0.0001$ – Figure 4B), yielding a TBR of 4.69.

We also imaged a patient with low grade squamous intraepithelial lesion (LSIL/CIN1), an abnormal proliferation of immature squamous cells involving no greater than the lower third of the squamous mucosa (Fig.5). Hand-held confocal microscopy of PARPi-FL showed organized tissue, with cells arranged in layers, but with nuclei of different sizes and shapes (Fig. 5A). H&E staining showed a similar finding in the CIN1, with nuclei of

varying sizes and shapes. PARP1 expression, and thus PARPi-FL uptake, was higher in the areas corresponding to disorganized tissue when compared to the healthy deeper stroma tissue. As usual in patients harboring CIN, this patient proved to be HPV positive (Fig. 5B).

To demonstrate that the technique could also be used to image tumor cells in different gynecological subsites, one patient with a recurrent squamous cell carcinoma of the vulva invading the clitoris was imaged. The clitoris biospecimen was imaged using the same rapid staining protocol and imaging protocol and the results were similar to the ones seen in the cervical cone biopsies: tumor presented with enlarged, variably-sized nuclei arranged in a disorganized manner, whereas the benign clitoral squamous mucosa (comprising the vast majority of the resected tissue) showed no PARPi-FL uptake (Fig 6A). Histology and PARP1 IHC corroborated the confocal findings, demonstrating that areas with no PARPi-FL signal corresponded to normal tissue, while areas with nuclear signal corresponded to tumor (Fig. 6B). The quantification of PARPi-FL fluorescence signal was significantly ($p < 0.0001$) higher in the tumor area (98.07 ± 18.78 a.u.) when compared to the normal surrounding tissue (19.49 ± 11.97), yielding a to a tumor to background fluorescence ratio of 5.03.

Discussion

PARP1 is an interesting target for tumor detection and delineation because of its increased expression in a large number of cancers types (23). Cancer is usually marked

by genomic instability that is often the result of alterations in the signaling of the DNA repair chain (24). Several clinical trials are investigating the use of PARP inhibitors in different types of tumors with promising results (12, 25-27). Although no cutoff has been previously reported determining when a lesion should be considered neoplastic by means of PARP1 expression, several papers have demonstrated that its increased expression can be used to differentiate tumors from their benign surrounding tissues (17, 23, 28, 29). Similar to what has been previously published for other malignancies (15, 17, 30-32), PARP1 is overexpressed in cervical adenocarcinomas. The difference in the PARP-expression between tumor and benign tissue was so marked that tumor could be delineated soley based on PARP quantification. Some tissues have physiologic PARP1 expression, especially those with high cellular turnover, such as the cervical squamous epithelium at the transformation zone. Thus, we have demonstrated that, even though the cervical squamous mucosa has higher PARP1 expression compared to stroma, it is significantly lower than in tumor. In this study, due to the low number of individuals, we did not consider the HPV status of patients for the purpose of imaging.

The ratio of PARP1 expression between tumor and normal allowed visualization of cervical cancer cells, after staining with a fluorescent tagged PARP1 inhibitor - PARPi-FL, using a hand-held confocal microscope. We demonstrate, using ex vivo fresh cone biopsies, that topical application of PARPi-FL on cervix is feasible, is capable of identifying tumor cells, and could potentially lead to a novel diagnostic tool for fast tumor cell identification, allowing imaging of cervical cancer in real time.

In vivo confocal microscopy has been of great interest since it allows for visualization of abnormal tissue without the need of an incisional biopsy. Both

fluorescence and reflectance confocal microscopy technologies are being studied in several other malignancies. We describe the use of a hand-held fluorescence microscope equipped with a blue laser (excitation: 488, emission: > 510), to detect the fluorescence signal arising from a contrast agent, PARPi-FL, that is specifically bound to PARP1 overexpressed in cancer cells. It is important to emphasize that PARPi-FL signal is in the green spectrum and autofluorescence emission is also a component of that same spectrum. The broader autofluorescence peak width, however, allows us to separate specific (PARPi-FL) and non-specific (autofluorescence) emissions. To achieve specific imaging, autofluorescence was being filtered using a band pass filter (515 nm – 575 nm). PARPi-FL is able to maintain target affinity once it has been modified on the cyclopropane end of the Olaparib scaffold, region that is not essential for binding (33-35). Dyes in the near infrared spectrum, were previously investigated and reported, but didn't achieve similar binding. (36, 37)

Taking advantage of the PARP1 expression in the basal layer of cervical squamous epithelium, we confirmed, using a swine animal model, that PARPi-FL penetrates into the tissue when applied topically. With minimal effort and time, its signal was detected by the hand-held confocal microscope allowing its use to obtain cellular resolution of the porcine cervix. As expected, the nuclei of normal tissue were considerably organized with homogeneous size and shape. When imaging cone biopsies with tumor, PARPi-FL showed higher uptake in lesions compared to surrounding normal tissue (Fig. 4 and 5), corresponding to PARP1 IHC expression in those areas. The tumors cells showed a disorganized pattern and heterogeneously shaped nuclei, which was easily discernible through PARPi-FL staining.

In addition, we found PARPi-FL uptake in CIN 1, which is not surprising since PARP1 expression is not only present in the basal layer, but also in squamous dysplasia (15). Importantly, different grades of cervical dysplasia are defined by the amount of immature squamous cell proliferation involving the mucosal thickness (CIN 1- involving one-third of the thickness, CIN 2 - one-third to two-thirds and CIN 3 - more than two-thirds of the epithelial layer). Confocal microscopy picks up the fluorescent signal that arises from one layer of cells (the XY-plane), which is ideal for cellularly resolving that layer and confirming specificity of the probe. However, unless depth is considered as well (the Z-plane) differentiating the grades of cervical dysplasia might be impractical. An associated technology, such as a hand-held epifluorescence tool, that could integrate fluorescence arising from the total thickness of the dysplastic area would be a promising asset for distinguishing between the different grades of CIN and tumor. Additionally, PARPi-FL could be used to assess suspicious lesions in real time or potentially replace acetic acid, serving as a more precise guide for biopsies or replace the need to biopsy.

Lastly, although further studies are necessary to define sensitivity and specificity of the tracer, our data suggests that PARPi-FL would work well for cancer screening during colposcopy procedures. It could also play a role in intraoperative imaging as a guide for tumor resection margins during LEEP / cone procedures as current approaches to determine the tumor boundaries rely on the expertise of the surgeon and ultimately final pathology. To date, no technology allows in vivo histology of cervical lesions, also no intraoperative tumor marker is available to ensure clear margins, resulting in additional procedures should positive margins be found on final pathology reports.

Conclusion

Contemporaneous and specific cellular visualization of cervical and clitoral cancer tissue was achieved using a topically applied fluorescent contrast agent, PARPi-FL, and a hand-held fluorescence confocal microscope. This tracer has the potential to improve tumor identification on colposcopy examination by allowing real time histology assessment.

Author Contributions

P.D.S.F., E.J. and T.R. conceived the study and designed the experiments. S.R. performed synthesis of PARPi-FL. P.D.S.F, N.G., A.R.K, S.K. and G.P. carried out the experiments and collected the data. P.D.S.F., K.P., E.J., A.M., and T.R analyzed the data. P.D.S.F. N.G. and T.R wrote animal protocols. P.D.S.F, N.G., E.J. and T.R wrote the IRB biospecimen protocol. P.D.S.F., A.M.; S.P., M.A., and T.R. conducted statistical analysis of the data. P.D.S.F., G.P., and T.R. primarily wrote the manuscript. All authors carefully read and edited the manuscript.

Data and materials availability. All data associated with this study are present in the paper or the Supplementary Materials.

Competing Interests. S.K., S.P. and T.R. are shareholders of Summit Biomedical Imaging, LLC. S.K., S.P. and T.R. are co-inventors on filed U.S. patent (WO2016164771) that covers methods of use for PARPi-FL. T.R. is co-inventor on U.S. patent (WO2012074840), covering the composition of matter for PARPi-FL. T.R. is a paid consultant for Theragnostics, Inc. All the other authors have no conflict to declare. This

arrangement has been reviewed and approved by Memorial Sloan Kettering Cancer Center in accordance with its conflict of interest policies.

Acknowledgements

The authors gratefully acknowledge the support of the Memorial Sloan Kettering Cancer Center's Animal Imaging Core Facility, the Radiochemistry & Molecular Imaging Probes Core, the Molecular Cytology Core, the Memorial Sloan Kettering Center for Molecular Imaging & Nanotechnology and the animal necropsy core at MSK. We also thank Garon Scott for editing the manuscript and Dr. Christian Brand and Dr. Gary Peterson for helpful discussions.

Key Points

Question. Can the difference in PARP1 expression between tumor and normal tissue, and therefore PARPi-FL uptake, be observed when imaging cervical lesions?

Pertinent Findings. PARPi-FL is a topical fluorescent tracer that targets the PARP1 enzyme in the DNA repair chain, overexpressed in cervical adenocarcinoma. After topical application, PARPi-FL signal could be picked up by a hand-held confocal microscope allowing cellular resolution of cervical lesions.

Implications for Patient Care. PARPi-FL signal can be picked up by a hand-held confocal microscope allowing cellular resolution of those lesions, we believe our tracer has a translational potential and could offer advantages to the current standard of care.

Bibliography

1. Ferlay J, Colombet M, Soerjomataram I, Mathers C, Parkin DM, Pineros M, et al. Estimating the global cancer incidence and mortality in 2018: GLOBOCAN sources and methods. International journal of cancer. 2019;144(8):1941-53.

2. Brisson M, Kim JJ, Canfell K, Drolet M, Gingras G, Burger EA, et al. Impact of HPV vaccination and cervical screening on cervical cancer elimination: a comparative modelling analysis in 78 low-income and lower-middle-income countries. Lancet (London, England). 2020.

3. Devarapalli P, Labani S, Nagarjuna N, Panchal P, Asthana S. Barriers affecting uptake of cervical cancer screening in low and middle income countries: A systematic review. Indian journal of cancer. 2018;55(4):318-26.

4. Toliman PJ, Kaldor JM, Tabrizi SN, Vallely AJ. Innovative approaches to cervical cancer screening in low- and middle-income countries. Climacteric : the journal of the International Menopause Society. 2018;21(3):235-8.

5. Parra SG, Rodriguez AM, Cherry KD, Schwarz RA, Gowen RM, Guerra LB, et al. Low-cost, high-resolution imaging for detecting cervical precancer in medically-underserved areas of Texas. Gynecologic oncology. 2019;154(3):558-64.

6. Parra S, Carranza E, Coole J, Hunt B, Smith C, Keahey P, et al. Development of Low-Cost Point-of-Care Technologies for Cervical Cancer Prevention Based on a Single-Board Computer. IEEE journal of translational engineering in health and medicine. 2020;8:4300210.

7. Pierce MC, Guan Y, Quinn MK, Zhang X, Zhang WH, Qiao YL, et al. A pilot study of low-cost, high-resolution microendoscopy as a tool for identifying women with cervical precancer. Cancer prevention research (Philadelphia, Pa). 2012;5(11):1273-9.

8. Mariano VS, Lorenzi AT, Scapulatempo-Neto C, Stein MD, Resende JC, Antoniazzi M, et al. A Low-Cost HPV Immunochromatographic Assay to Detect High-Grade Cervical Intraepithelial Neoplasia. PloS one. 2016;11(10):e0164892.

9. Rodriguez NM, Wong WS, Liu L, Dewar R, Klapperich CM. A fully integrated paperfluidic molecular diagnostic chip for the extraction, amplification, and detection of nucleic acids from clinical samples. Lab on a chip. 2016;16(4):753-63.

10. Catarino R, Schafer S, Vassilakos P, Petignat P, Arbyn M. Accuracy of combinations of visual inspection using acetic acid or lugol iodine to detect cervical precancer: a meta-analysis. BJOG : an international journal of obstetrics and gynaecology. 2018;125(5):545-53.

11. Parham GP, Mwanahamuntu MH, Kapambwe S, Muwonge R, Bateman AC, Blevins M, et al. Population-level scale-up of cervical cancer prevention services in a low-resource setting: development, implementation, and evaluation of the cervical cancer prevention program in Zambia. PloS one. 2015;10(4):e0122169.

12. Boussios S, Karihtala P, Moschetta M, Karathanasi A, Sadauskaite A, Rassy E, et al. Combined Strategies with Poly (ADP-Ribose) Polymerase (PARP) Inhibitors for the Treatment of Ovarian Cancer: A Literature Review. Diagnostics (Basel). 2019;9(3).

13. Pujade-Lauraine E, Ledermann JA, Selle F, Gebski V, Penson RT, Oza AM, et al. Olaparib tablets as maintenance therapy in patients with platinum-sensitive, relapsed ovarian cancer and a BRCA1/2 mutation (SOLO2/ENGOT-Ov21): a double-blind,

randomised, placebo-controlled, phase 3 trial. The Lancet Oncology. 2017;18(9):1274-84.

14. Kossatz S, Weber WA, Reiner T. Optical Imaging of PARP1 in Response to Radiation in Oral Squamous Cell Carcinoma. PloS one. 2016;11(1):e0147752.

15. Kossatz S, Pirovano G, Demetrio De Souza Franca P, Strome AL, Sunny SP, Zanoni DK, et al. Validation of the use of a fluorescent PARP1 inhibitor for the detection of oral, oropharyngeal and oesophageal epithelial cancers. Nature biomedical engineering. 2020;4(3):272-85.

16. Chow JP, Man WY, Mao M, Chen H, Cheung F, Nicholls J, et al. PARP1 is overexpressed in nasopharyngeal carcinoma and its inhibition enhances radiotherapy. Mol Cancer Ther. 2013;12(11):2517-28.

17. Demetrio de Souza Franca P, Roberts S, Kossatz S, Guru N, Mason C, Zanoni DK, et al. Fluorine-18 labeled poly (ADP-ribose) polymerase1 inhibitor as a potential alternative to 2-deoxy-2-[(18)F]fluoro-d-glucose positron emission tomography in oral cancer imaging. Nuclear medicine and biology. 2020;84-85:80-7.

18. Kossatz S, Brand C, Gutiontov S, Liu JT, Lee NY, Gonen M, et al. Detection and delineation of oral cancer with a PARP1 targeted optical imaging agent. Scientific reports. 2016;6:21371.

19. Thurber GM, Yang KS, Reiner T, Kohler RH, Sorger P, Mitchison T, et al. Single-cell and subcellular pharmacokinetic imaging allows insight into drug action in vivo. Nat Commun. 2013;4:1504.

20. Carney B, Kossatz S, Reiner T. Molecular imaging of PARP. Journal of Nuclear Medicine. 2017;58(7):1025-30.

21. Zhu W, Pirovano G, O'Neal PK, Gong C, Kulkarni N, Nguyen CD, et al. Smartphone epifluorescence microscopy for cellular imaging of fresh tissue in low-resource settings. Biomedical optics express. 2020;11(1):89-98.

22. Reiner T, Lacy J, Keliher EJ, Yang KS, Ullal A, Kohler RH, et al. Imaging therapeutic PARP inhibition in vivo through bioorthogonally developed companion imaging agents. Neoplasia (New York, NY). 2012;14(3):169-77.

23. Tang J, Salloum D, Carney B, Brand C, Kossatz S, Sadique A, et al. Targeted PET imaging strategy to differentiate malignant from inflamed lymph nodes in diffuse large B-cell lymphoma. Proceedings of the National Academy of Sciences of the United States of America. 2017;114(36):E7441-e9.

24. Mateo J, Lord CJ, Serra V, Tutt A, Balmaña J, Castroviejo-Bermejo M, et al. A decade of clinical development of PARP inhibitors in perspective. Ann Oncol. 2019;30(9):1437-47.

25. Wilson RH, Evans TJ, Middleton MR, Molife LR, Spicer J, Dieras V, et al. A phase I study of intravenous and oral rucaparib in combination with chemotherapy in patients with advanced solid tumours. Br J Cancer. 2017;116(7):884-92.

26. Litton JK, Rugo HS, Ettl J, Hurvitz SA, Gonçalves A, Lee KH, et al. Talazoparib in Patients with Advanced Breast Cancer and a Germline BRCA Mutation. The New England journal of medicine. 2018;379(8):753-63.

27. Clarke N, Wiechno P, Alekseev B, Sala N, Jones R, Kocak I, et al. Olaparib combined with abiraterone in patients with metastatic castration-resistant prostate cancer: a randomised, double-blind, placebo-controlled, phase 2 trial. The Lancet Oncology. 2018;19(7):975-86.

28. Schoder HM, Demetrio De Souza Franca P, Nakajima R, Burnazi EM, Roberts S, Brand C, et al. Safety and feasibility of PARP1/2 imaging with 18F-PARPi in patients with head and neck cancer. Clinical cancer research : an official journal of the American Association for Cancer Research. 2020; 26:3110-3116.

29. Pirovano G, Jannetti SA, Carter LM, Sadique A, Kossatz S, Guru N, et al. Targeted Brain Tumor Radiotherapy Using an Auger Emitter. Clinical cancer research : an official journal of the American Association for Cancer Research. 2020;26(12):2871-81.

30. Carney B, Kossatz S, Lok BH, Schneeberger V, Gangangari KK, Pillarsetty NVK, et al. Target engagement imaging of PARP inhibitors in small-cell lung cancer. Nature communications. 2018;9(1):176.

31. Zhou D, Xu J, Mpoy C, Chu W, Kim SH, Li H, et al. Preliminary evaluation of a novel (18)F-labeled PARP-1 ligand for PET imaging of PARP-1 expression in prostate cancer. Nuclear medicine and biology. 2018;66:26-31.

32. Pirovano G, Jannetti SA, Carter LM, Sadique A, Kossatz S, Guru N, et al. Targeted brain tumor radiotherapy using an Auger emitter. Clinical cancer research : an official journal of the American Association for Cancer Research. 2020; 26:2871-2881.

33. Carney B, Kossatz S, Reiner T. Molecular Imaging of PARP. Journal of nuclear medicine : official publication, Society of Nuclear Medicine. 2017;58(7):1025-30.

34. Dubach JM, Kim E, Yang K, Cuccarese M, Giedt RJ, Meimetis LG, et al. Quantitating drug-target engagement in single cells in vitro and in vivo. Nature chemical biology. 2017;13(2):168-73.

35. Dubach JM, Vinegoni C, Mazitschek R, Fumene Feruglio P, Cameron LA, Weissleder R. In vivo imaging of specific drug-target binding at subcellular resolution. Nature communications. 2014;5:3946.

36. Thurber GM, Reiner T, Yang KS, Kohler RH, Weissleder R. Effect of small-molecule modification on single-cell pharmacokinetics of PARP inhibitors. Mol Cancer Ther. 2014;13(4):986-95.

37. Demétrio de Souza França P, Guru N, Roberts S, Kossatz S, Mason C, Abrahão M, et al. Fluorescence-guided resection of tumors in mouse models of oral cancer. Scientific reports. 2020;10(1):11175.

Figures

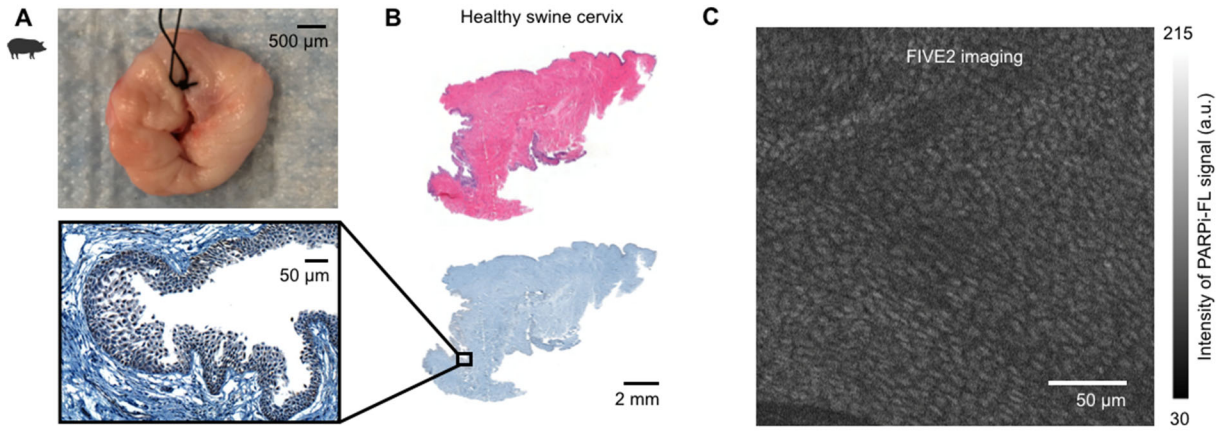

Fig. 1. PARPi-FL imaging on a healthy swine cervix. Physiological PARP1 expression in cervical squamous basal layer allowed confocal imaging of healthy tissue in swine. (A) A cone biopsy was obtained from three swine and stained with PARPi-FL. (B) H&E with corresponding IHC demonstrating the presence of PARP1. (C) Hand-held confocal microscopy shows cells arranged in layers with nuclei of the same size and shape. Tissue depth 10 µm.

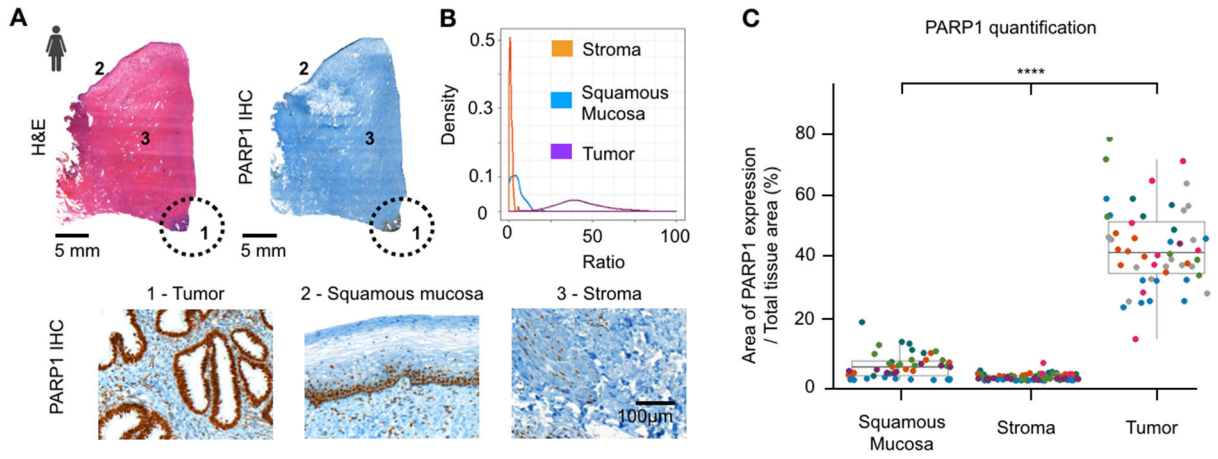

Fig. 2. PARP1 expression on human cervical cancer banked tissue. (A) Tumor (cervical adenocarcinomas) and normal areas on H&E and IHC patient slides. The circle demarcates the tumor. IHC shows that PARP1 is highly expressed in adenocarcinoma whereas it is much lower in the normal stroma of benign squamous epithelium. (B) Density of the ratio value according to tissue type (x-axis truncated at 100 for visibility purpose). (C) Distribution of the ratio value according to tissue type (10 higher extremes values in the Tumor group were excluded for visibility purposes). Each color in the graph represents a different patient (n = 7). *$p < 0.05$, **$p < 0.01$, ** $p < 0.001$. Data in (C) are presented as mean ± s.d.

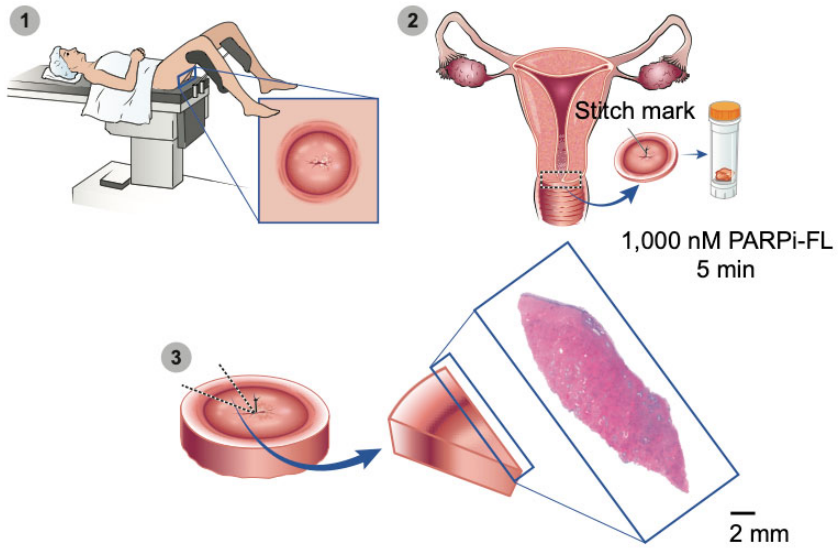

Fig. 3. Experimental plan for patient's cone biopsy biospecimen collection. 1 - Cone biopsies from patients were resected and evaluated in the operating room, before the standard of care processing. 2 - Staining was carried out on the whole, freshly excised specimen by submersing the tissue in a solution containing 1000 nM PARPi-FL solution in 15 mL of 30% PEG 300 in PBS for 5 minutes (rapid staining protocol). The specimen was further washed in PBS for 1 min prior to imaging. 3 - After imaging, the specimens were processed according to the standard of care. The gynecological pathologist confirmed the histological results and provided slides for the study. The magnified image demonstrates how the pathology slides were acquired.

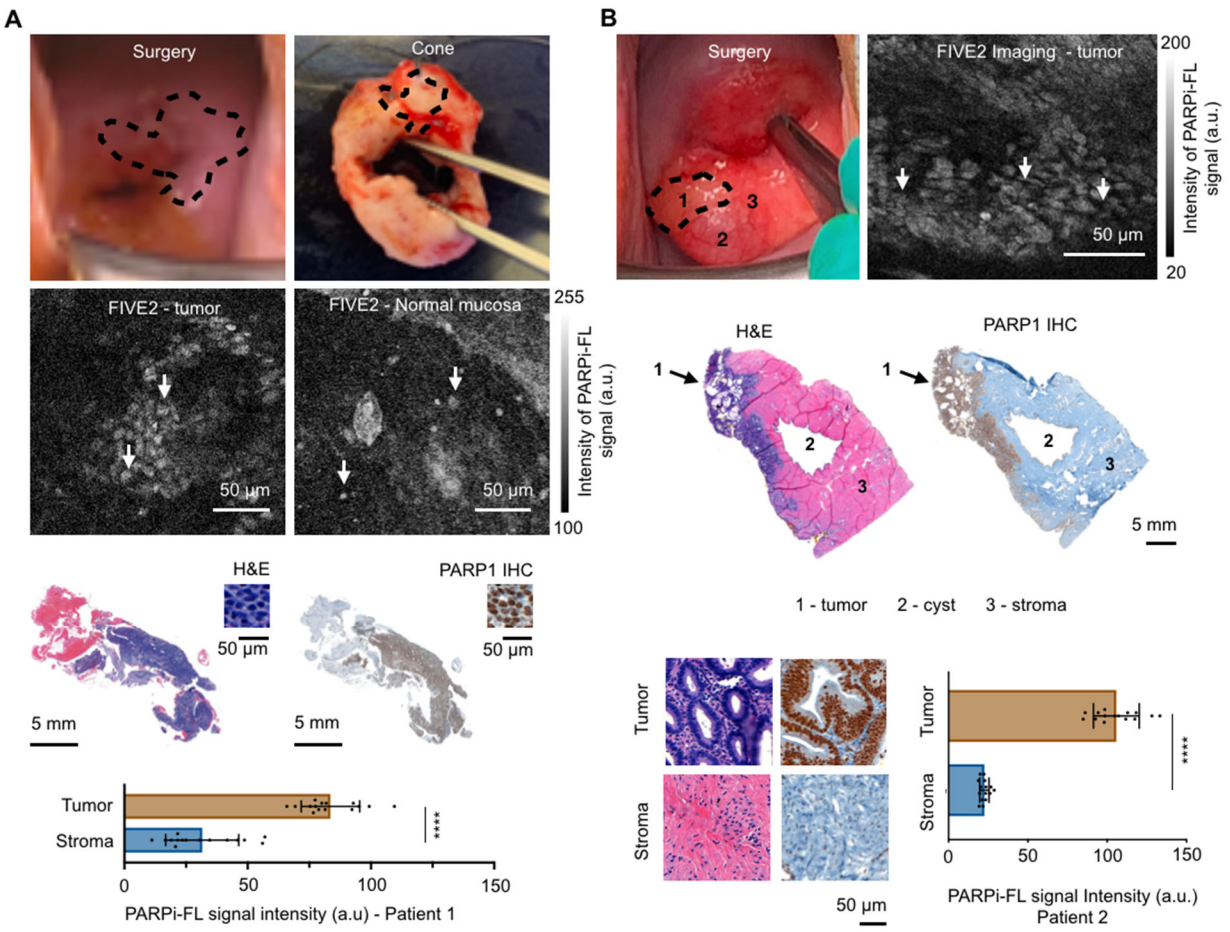

Fig. 4. PARPi-FL imaging of cervical cancer. Patients imaged with PARPi-FL stain and a hand-held confocal imaging in the OR, prior to final pathology report for the standard of care. (A) Patient 1 harbored an adenocarcinoma of the cervical transformation zone, extending to the ectocervical mucosa – dotted lines represent tumor delineation. The second-row shows tumor and healthy mucosa imaged by the hand-held confocal microscope, depth in the tissue 13 µm, and 8 µm respectively. Images show cells arranged in a disorganized manner and nuclei with different sizes and shapes, arrows point to cell nuclei (average intensity signal 83.57 ± 11.85 a.u.). Normal mucosa shows

almost no PARPi-FL uptake (average intensity signal 22.53 ± 2.94 a.u.). Sparse and regularly shaped nuclei were observed (arrows). H&E and PARP1 IHC slides show areas of tumor with increased PARP1 expression. Almost no PARP1 expression is present in the normal tissue area. (B) Patient 2 harbored a cervical adenocarcinoma, represented in the dotted lines, located adjacent to a benign Nabothian cyst. Numbers represent 1 – tumor, 2 – cyst, 3 – Normal stroma. Tissue depth 3 μm. PARPi-FL in tumor emitted a significantly higher signal than in the normal surrounding mucosa (105.8 ± 14.45 a.u., 22.53 ± 2.94 a.u., respectively, $p < 0.0001$). H&E and PARP1 IHC staining confirmed the presence of tumor. `

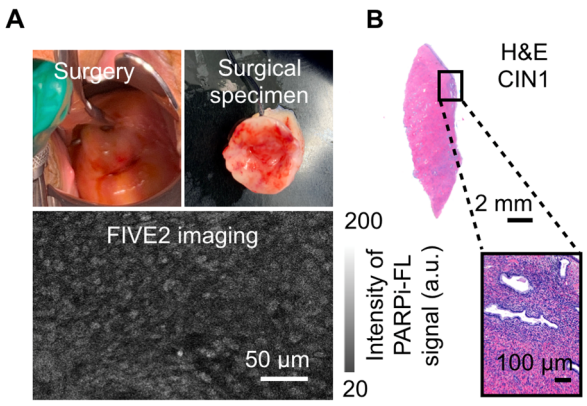

Fig. 5. PARPi-FL imaging of cervical dysplasia. Patient imaged with PARPI-FL stain and a hand-held confocal imaging in the OR, prior to the final pathology report. Standard of care assessment. (A) The patient harbored a cervical intraepithelial neoplasia type 1 (CIN1) of the cervical os. Images from the lesion demonstrated cells arranged in a slightly disorganized manner with nuclei of different sizes and shapes. Image depth: 4 μm. (B) Overview of the specimen and magnified. The square represents the magnified image.

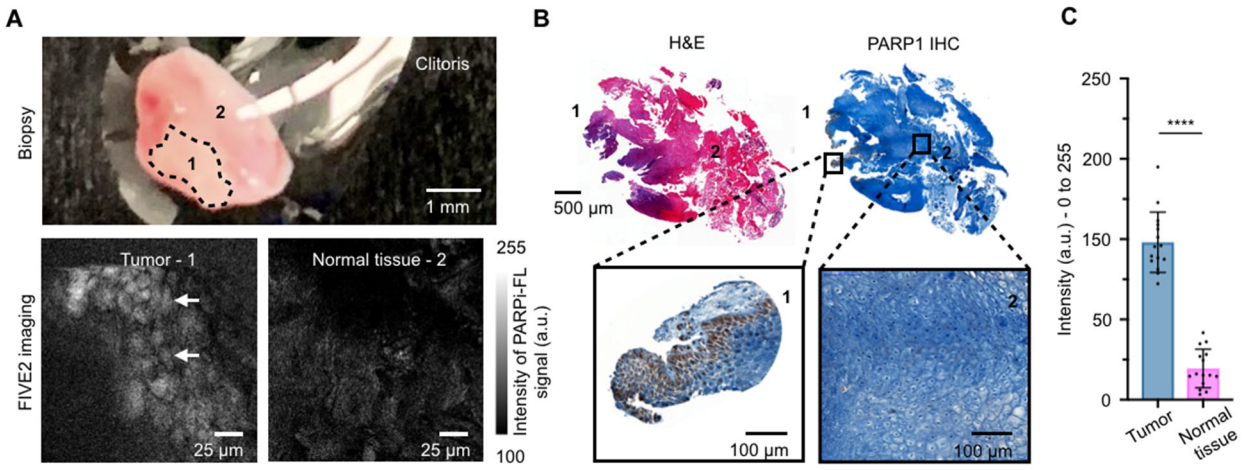

Fig. 6. PARPi-FL imaging of a clitoral excision – invasion from a vulvar squamous cell carcinoma. Imaging with PARPi-FL was also carried out in one patient harboring a recurrent squamous cell carcinoma of the vulva invading the clitoris. (A) Patient biospecimen ex vivo. The dotted area (1) corresponds to the tumor and the surrounding area (2) corresponds to benign margins. Bottom row: Images acquired with the hand-held confocal microscope demonstrated tumor cells with enlarged nuclei that were different in size and arranged in a very disorganized manner. Tissue depth 4 µm (tumor) and 6 µm (normal tissue). (B) H&E staining showed that the tumor was restricted to a small area in the tissue – represented by number 1. PARP1 IHC corroborated the confocal findings since no PARP1 expression was present in the stroma (2) whereas it was present in tumor (1). (C) Quantification of PARPi-FL uptake in tumor and normal tissue. Fluorescence signal was significantly ($p < 0.0001$) higher in the tumor area when compared to the normal surrounding tissue.

SUPPLEMENTARY INFORMATION FOR:

PARP1: A potential molecular marker to identify cancer during colposcopy procedures.

Paula Demétrio De Souza França[1,2], Navjot Guru[1], Abigail R. Kostolansky[1,3], Audrey Mauguen[4], Giacomo Pirovano[1], Susanne Kossatz[1,5], Sheryl Roberts[1], Marcio Abrahão[2], Snehal G. Patel[6], Kay J. Park[7], Thomas Reiner[1,8,9,*], Elizabeth Jewell[6,*]

[1] Department of Radiology, Memorial Sloan Kettering Cancer Center, New York, NY, USA.

[2] Department of Otorhinolaryngology and Head and Neck Surgery, Federal University of São Paulo, SP, Brazil.

[3] Department of Chemistry, Princeton University, Princeton, NJ, USA.

[4] Department of Epidemiology and Biostatistics, Memorial Sloan Kettering Cancer Center, New York, NY, USA.

[5] Department of Nuclear Medicine, University Hospital Klinikum Rechts der Isar and TranslaTUM, Technical University Munich, Munich, Germany

[6] Department of Surgery, Memorial Sloan Kettering Cancer Center, New York, NY, USA.

[7] Department of Pathology, Memorial Sloan Kettering Cancer Center, New York, NY, USA.

[8] Department of Radiology, Weill Cornell Medical College, New York, NY, USA.

[9] Chemical Biology Program, Memorial Sloan Kettering Cancer Center, New York, NY, USA.

*EJ and TR contributed equally as co-senior authors

Tables.

Tissue	N (measures)	N (patients)	Mean	SD	Median	Min	Max
Epithelium	46	5	4.62	3.94	4.37	0.16	18.48
Normal	83	7	1.08	0.91	0.82	0.03	5.58
Tumor	63	7	69.82	64.42	44.49	13.20	263.02

Table 1. Data description. PARP1 expression in three tissue areas: epithelium, normal tissue and tumor. The numbers represent measures of the percentage of PARP1 expression on those different areas (% of PARP1 expression over the total tissue area, data also represented on Fig. 1B and C). Note that 2 patients had no measurements in the epithelium since no healthy epithelium could be found on the specimen.

	Predicted average value			
N = 192		**Coefficient**	**95% CI**	**p-value (against tumor expression)**
Tissue				
Tumor	59.6	1.00 (Ref.)		
Epithelium	3.0	0.05	0.04, 0.07	<0.001
Margin	0.7	0.01	0.009, 0.015	<0.001

Table 2. Linear regression accounting for the repeated measurements per patients. The linear regression was done on the logarithm transformation of the ratio (to ensure no negative prediction). The table presents the results transformed back to the original scale, and coefficients are multiplicative. When accounting for the repeated measurements per patients (with a random intercept), the ratio is on average reduced by 95% in epithelium as compared to tumor, and by 99% in normal as compared to tumor. The ratio in normal tissue is on average 77% lower than epithelium (95%CI: 0.18 to 0.30, $p < 0.001$).